Journal of ELECTRONIC MATERIALS, Vol. 45, No. 1, 2016
DOI: 10.1007/s11664-015-4150-5
© 2015 The Minerals, Metals & Materials Society

CrossMark

Influence of Substrate Temperature on the Properties of Nanostructured ZnO Thin Films Grown by RF Magnetron Sputtering

H. MAHDHI,[1,4] Z. BEN AYADI,[1] J. L. GAUFFIER,[3] and K. DJESSAS[2]

1.—Laboratoire de Physique des Matériaux et des Nanomatériaux Appliquée à l'Environnement, Faculté des Sciences de Gabès, Cité Erriadh Manara Zrig, 6072 Gabès, Tunisia. 2.—Laboratoire Procédés, Matériaux et Energie Solaire (PROMES-CNRS), Université de Perpignan, Rambla de la Thermodynamique, Tecnosud, 66100 Perpignan Cedex, France. 3.—Département de Physique, INSA de Toulouse, 135 Avenue de Rangueil, 31077 Toulouse Cedex 4, France. 4.—e-mail: hayetmahdhi@yahoo.fr

Transparent conducting thin films of ZnO:Ga (GZO) have been deposited onto glass substrates and were prepared by RF-magnetron sputtering from nanoparticles synthesized by the sol–gel method. The preheated substrate temperature was changed from room temperature to 300°C. X-ray diffraction spectra showed that the as-deposited films are polycrystalline ZnO with a hexagonal wurtzite structure. Surface morphology, optical properties (such as transmission, reflectance), and conductivity were investigated. The obtained results revealed that the structures and properties of the films were greatly affected by the substrate temperature. Thin films of GZO have a low resistivity, with a minimum value of 2.20×10^{-3} Ω cm deposited at a substrate temperature of 200°C.

Key words: Zinc oxide, nanostructure, RF-magnetron sputtering, substrate temperature, optical and electrical properties

INTRODUCTION

Transparent conducting zinc oxide films have been extensively studied in recent years, because of their low cost precursor materials, relatively low deposition temperature and high stability in hydrogen plasma compared to oxide tin indium (ITO) and dioxide tin (SnO_2) films.[1] These advantages are of considerable interest for solar energy conversion applications. The high chemical and thermal stability and high abundance of zinc oxide make it an attractive material for a wide variety of applications, such as ultraviolet (UV) emitters and detectors,[2] light-emitting devices,[3,4] gas sensors,[5,6] surface acoustic wave devices[7] and transparent electrodes.[8,9] Doped zinc oxide materials have been extensively studied, because of their remarkable optical and electrical properties. The mechanisms of doping may be deviating from the stoichiometry of ZnO, mainly by the introduction of excess zinc atoms in interstitial position, or by the creation of oxygen vacancies (the centers created then behave as electron donors),[10] or by substituting zinc atoms or oxygen atoms by foreign network different valence. The addition of Group III metal dopants, such as Al, In and Ga, increases the electrical conductivity and transparency of ZnO films. The incorporation of these elements into the ZnO lattice can stabilize the film at high temperatures, and increase its electrical conductivity.[11] Among these elements, Ga is the most effective n-type dopant in ZnO since the ionic and the covalent radii (0.62 Å and 1.26 Å) are closer to those of Zn (0.74 Å and 1.31 Å) and the covalent bond length of Ga-O (1.92 Å) is also closely matched with that of Zn-O (1.97 Å).[12,13]

Several techniques of deposition have been used for the production of ZnO thin films, such as evaporation,[14] chemical vapor deposition (CVD),[15,16]

(Received May 16, 2015; accepted October 13, 2015; published online November 6, 2015)

spray pyrolysis,[17] magnetron sputtering [18–20] and pulsed laser deposition (PLD).[21]

However, among these techniques, the sputtering and sol–gel processes offer many advantages. Sputtering performed at a high deposition rate, with no toxic gas emissions, is easy to expand to large-scale glass substrates with no undesired layer formation problems,[22] and is a low cost and simple method. On the other hand, the sol–gel technique emerged within the last two decades and quickly became one of the most important and promising new material fabrication methods. Indeed, besides the fact that it is a low cost technique, it enables researchers to easily design and fabricate a wide variety of different materials, including the possibility of doping even at high level concentrations at room temperature (RT). Compared with other techniques, the sol–gel method has many advantages such as low cost, simple synthesis equipment, easy fabrication of large areas, easier adjustment of composition, and being able to carry out doping at molecular level. It is especially suitable for the fabrication of oxide nanoparticles.[23] How to prepare high-quality ZnO nanoparticles by the sol–gel method has become a research subject for a comparison between the structural and optical properties of nanocrystalline ZnO nanopowder such as crystallite size and band gap energy.

In our previous research work, we developed a novel method to fabricate ZnO films as-deposited from ZnO nanostructures synthesized by the sol–gel technique.[24] Therefore, the structural properties of the obtained ZnO thin-films were partly dependent on the ZnO nanoparticles. Furthermore, the properties of the as-deposited ZnO films were partly dependent on the properties of the substrates, such as the crystal orientation, the conductivity, and the roughness. In the present work, a systematic investigation of the structural and optical properties of GZO films deposited by RF-magnetron sputtering at various substrate temperatures is reported using a nanocrystalline powder synthesized by the sol–gel method. The main purpose is to further understand the influence of substrate temperature on the optical properties of GZO films. In particular, optical parameters such as the optical band gap, Urbach energy, refractive index and electrical conductivity are investigated.

EXPERIMENTAL

ZnO:Ga nanocrystals were prepared by the sol–gel method using 10 g of zinc acetate dehydrate [$Zn(CH_3COO)$, $2H_2O$] as a precursor in 70 mL of methanol. After 10 min under magnetic stirring at RT, an adequate quantity of gallium nitrate [GaN_3O_9], corresponding to [Ga]/[Zn] = 0, 1, 3 and 5 at.% were added. After 10 min under magnetic stirring, the solution was placed in an autoclave and dried in a supercritical condition of ethanol (EtOH). Then, the GZO films were deposited on a glass substrate by RF-magnetron sputtering (13.56 MHz-Cezar RF-power Generator). Before each deposition, the sputter chamber was evacuated to a base pressure of about 10^{-5} mbar. After introducing the sputtering in argon gas with 99.9999% high purity without oxygen, the sputtering deposition was carried out at a pressure of 10^{-3} mbar. The sputtering targets were prepared from the aerogel powders of ZnO:Ga. During the sputtering process, the RF power was 60 W and the substrate temperature was between RT and 300°C. Before deposition of the GZO thin films, the glass substrates with 1 mm thickness were ultrasonically cleaned in HCl, rinsed in deionized water, then subsequently in ethanol and rinsed again.

The crystal structure was characterized by x-ray diffraction (XRD) using CuKα radiation (1.5406 Å). The crystallite size was calculated from XRD data using Scherrer's formula.[25]

$$G = \frac{0.9\lambda}{\beta \cos \theta_B}, \qquad (1)$$

where λ is the x-ray wavelength, θ is the Bragg diffraction angle and β is the FWHM of the XRD peak (in radians). The GZO nanoparticles were also characterized by transmission electron microscopy (TEM) using JEM-200CX. The composition studies were performed by energy dispersive x-ray spectroscopy (EDS) using a scanning electron microscope (SEM) JEOL JSM 5410 type with an EDS attachment. Surface morphology and roughness were measured using atomic force microscopy (AFM; Topo Metrix). Electrical resistivity, Hall mobility and carrier concentration were measured at RT by a Hall measurement system with the Van der Pauw method. The optical transmittance of the films was determined using a Shimadzu UV-3101 PC spectrophotometer in the wavelength range from 200 nm to 3000 nm.

RESULTS AND DISCUSSION

Structural and Morphological Properties

Figure 1 shows the evolution of diffraction patterns of x-rays aerogels nanoparticles ZnO:Ga synthesized by the sol–gel method at different concentrations of gallium. Five pronounced peaks appear at 2θ = 31.66°; 34.42°, 36.17°; 47.46° and 56.64°. They are provided from the planes (100), (002), (101), (102) and (110), respectively.[26] This result indicates that GZO aerogel powder has a polycrystalline hexagonal wurtzite structure. The average grain size of the basal diameter of the cylinder-shape crystallites varies from 14 nm to 20 nm, whereas the height of the crystallites varies from 25 nm to 34 nm.

The observations by TEM and SEM of the nanoparticles ZnO:Ga shows that the doped ZnO nanoparticles are fine with a prismatic shape and a narrow particle size distribution (Fig. 2). The size of

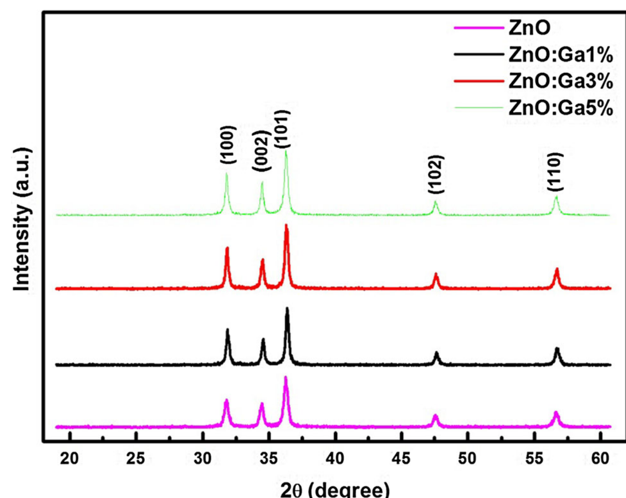

Fig. 1. X-ray patterns of ZnO:Ga aerogel nanoparticles for various gallium doping levels.

the majority of the nanoparticles of ZnO:Ga in this powder ranges from 20 nm to 30 nm. The morphology of all the samples is found to be nearly spherical in nature with the diameters ranging from 14 nm to 35 nm, in a good agreement with the results of the XRD. The chemical composition of ZnO:Ga nanoparticles performed by EDS are presented in Fig. 2b and compiled in Table I. The EDS analysis confirms the presence of gallium in the ZnO matrix with no other impurities. From this analysis, we can conclude that the ZnO nanoparticles doped with gallium are homogeneous and quasi-stoichiometric.

The XRD patterns of ZnO:Ga thin films deposited at RT with different Ga concentrations, and films deposited from a fixed concentration, [Ga/Zn] = 3 at.% and different deposition temperatures are shown in Fig. 3a and b, respectively. All films have hexagonal wurtzite structure. A prominent (002) peak indicates structure preferential orienta-

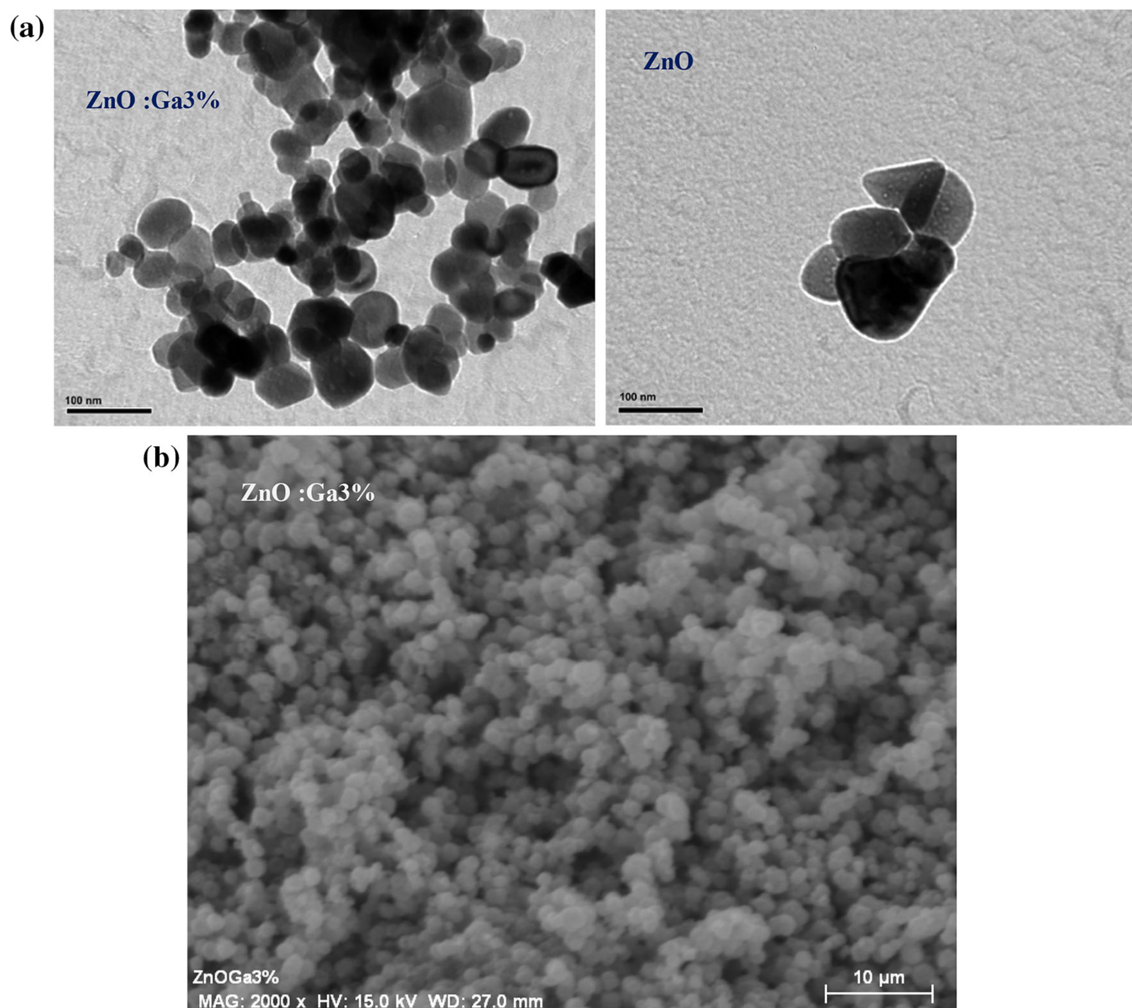

Fig. 2. Typical TEM photograph (a) and SEM showing (b) the general morphology of GZO aerogel nanoparticles.

Table I. Atomic compositions of GZO nanoparticles

Chemical composition	Zinc (at.%)	Oxygen (at.%)	Gallium (at.%)
ZnO	48.43	51.57	0.00
ZnO:Ga1%	46.82	52.81	0.37
ZnO:Ga3%	47.12	51.54	1.34
ZnO:Ga 5%	46.78	51.04	2.18

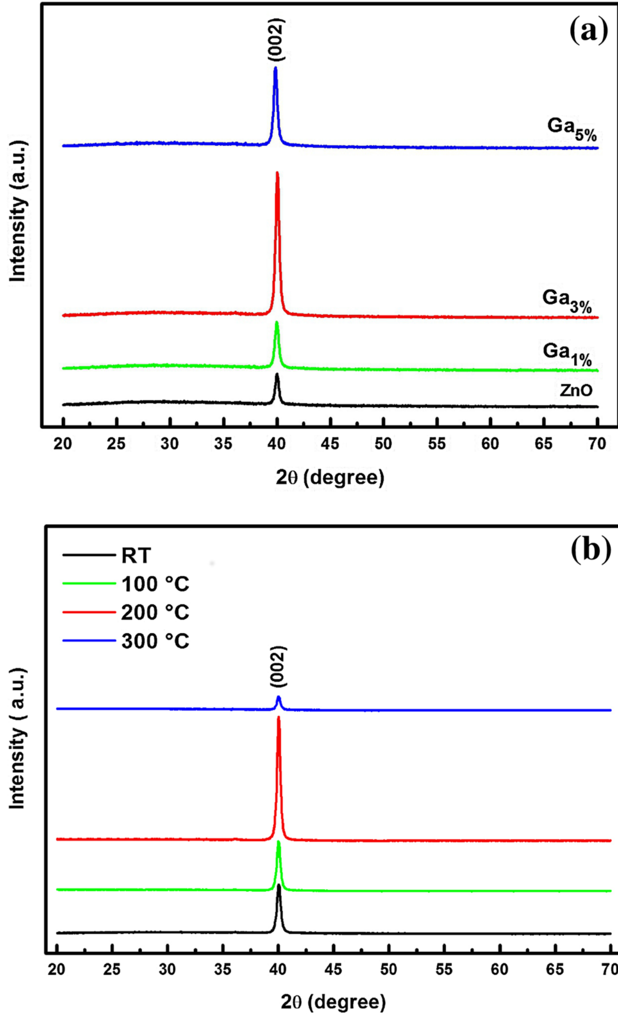

Fig. 3. XRD patterns of GZO films deposited on glass substrates with different Ga content (a) and the GZO3.0% thin films deposited at various substrate temperatures (b).

tion of the films with their c-axis perpendicular to the substrate plane.[27] The films are developed without any second phase, indicating that they have a high-quality crystalline structure. It has been established that the preferred orientation is a result of a self-ordering caused by the minimization of the crystal surface energy.[28] All Ga-doped ZnO thin films show high (002) diffraction peak intensity. This means that the as-deposited ZnO:Ga films show a good crystalline quality for gallium concentrations between 1.0 at.% and 5.0 at.%. The grain sizes for the films, calculated using Scherrer's formula, are comparable to those of the ZnO powder. The (002) peak intensity increases with the gallium concentration and reaches a maximum for a concentration of 3.0 at.% of Ga. However, the (002) diffraction peak intensity decreased with increasing doping concentrations over 3.0 at.%. This indicates that an increase in doping concentration above a critical value (3.0 at.%) causes a deterioration of the crystallinity of the films, which may be due to the formation of the stresses induced by the difference in ion size between zinc and the dopant[29] and the segregation of dopants in grain boundaries for high doping concentrations.

It is also clearly observed that the intensity of the (002) XRD peak increases with increasing the substrate temperature. On the other hand, a variation in the position of the (002) diffraction peak as a function of the substrate temperature is observed (Table II). As Ts increases from RT to 300°C, the average crystal size increases from 29.20 nm to 32.20 nm, indicating that a high substrate temperature can improve the crystallinity of the GZO film. The crystallite size increased with the increase of substrate temperature, but decreased slightly at 300°C.

The variation of crystallite size as a function of substrate temperature is shown in Fig. 4. A noticeable increase is seen in crystalline size with the substrate temperature. The larger grain size implies the improvement of the crystallinity of the films. From the XRD results, it can be concluded that the film properties are strongly dependent on substrate temperature. The lattice constant c can be calculated by the formula[30]:

$$d_{hkl} = \frac{a}{\sqrt{\frac{4}{3}(h^2 + k^2 + hk) + l^2 \frac{a^2}{c^2}}} \quad (2)$$

Table II. Variation of the (002) peak positions, FWHM, grain size, interreticular distance (d_{hkl}) and lattice parameters of GZO films deposited at various substrate temperatures

Substrate temperature (°C)	(002), 2θ (deg)	FWHM (deg.)	Grain size (nm)	d_{hkl} (nm)	c (Å)
RT	40.04	0.337	29.20	0.2615	5.230
100	40.00	0.326	30.10	0.2613	5.226
200	40.05	0.305	32.20	0.2612	5.224
300	40.04	0.338	29.06	0.2614	5.228

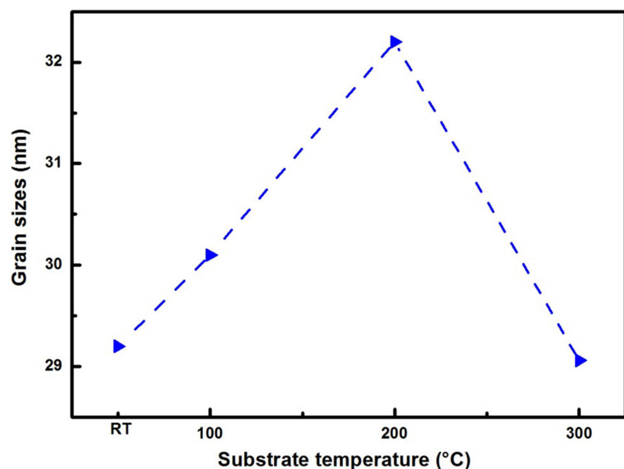

Fig. 4. Evolution of grain size of GZO 3.0 at.% thin films according to the substrate temperature.

where a and c are the lattice constants and d_{hkl} is the crystalline plane distance for indices (hkl). According to Eq. 2, the lattice constant c is equal to 2 d_{hkl} for the (002) diffraction peak. The values of d_{hkl} and c are listed in Table II. All the values of d_{hkl} are larger than that of standard ZnO powder (2.603 Å), indicating that the crystalline plane distances of GZO films are lengthened by imperfections such as lattice strains and interstitial defects. The XRD peak of GZO 3 at.% film is moved towards the larger θ values, which leads to a decrease in the lattice parameter c (Table II). This reduction is directly related to the incorporation of Ga^{+3} ions in substitutional sites Zn^{+2}. Then, the incorporation of the dopant in the ZnO matrix leads to a network contraction.

The substrate temperature dependence of the crystallite size for GZO films was also revealed by the AFM micrographs. Figure 5 shows the surface

Fig. 5. Surface morphologies for GZO 3.0 at.% films deposited at various substrate temperatures: (a) QT = RT, (b) T = 100°C, (c) T = 200°C and (d) T = 300°C.

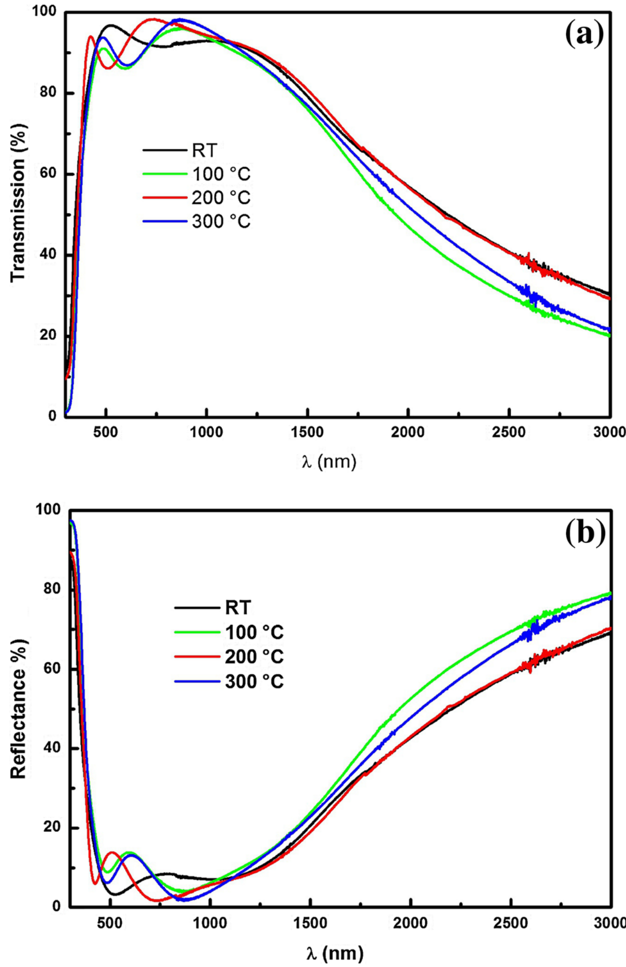

Fig. 6. Transmittance (a) and reflectance (b) spectra of GZO films deposited at various substrate temperatures.

morphologies of the films deposited at various substrate temperatures. An increase in grain size with temperature and a decrease in the roughness are observed. The roughness average values of these films varied in the range of ~3–8 nm; a higher deposition temperature resulted in rougher films.

Optical Studies

The optical transmittance and reflectance of ZnO:Ga 3 at.% (GZO 3 at.%) films deposited at different substrate temperatures, in the spectral range of 200–3000 nm, are shown in Fig. 6a and b. The observed interference fringes with deep valleys and tall crests indicate that the films have a smooth surface. The high transmission of all these samples demonstrates that ZnO thin films can be used as an optical window in optoelectronic devices. The steep drop of the transmission for the lower wavelengths at 380 nm corresponds to the absorption in ZnO due to the transition between the valence band and the conduction band. This area is used to determine the energy of the optical gap. According to the theoretical and practical calculations, the ZnO has a direct

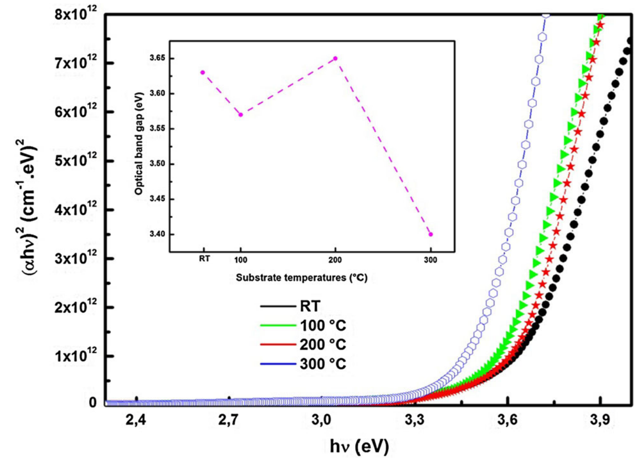

Fig. 7. Relationship between $(\alpha h\nu)^2$ and photo energy ($h\nu$) for GZO 3.0 at.% films deposited at various substrate temperatures.

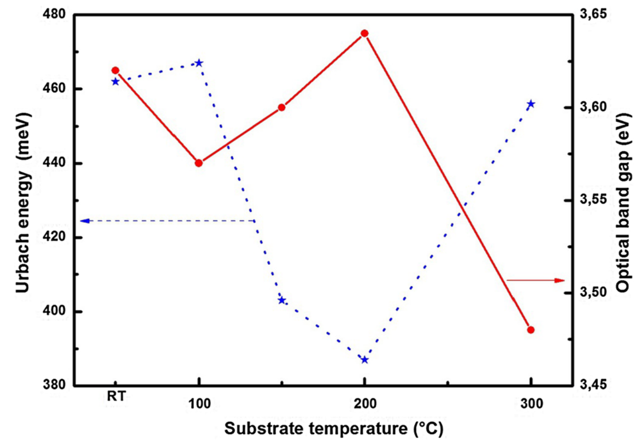

Fig. 8. Evolution of the energy gap and the Urbach energy depending on the temperature of the substrate.

inter-band transition[31] and for direct allowed transitions between the parabolic bands, the band gap of films was obtained by Tuac's relationship.[32]

$$\alpha(h\nu) = A(h\nu - E_g)^{1/2}, \quad (3)$$

where A is a constant for direct transition, and $h\nu$ is the energy of the incident photon.

The optical absorption coefficient (α) is calculated from the transmittance data, where the reflection losses are taken into consideration, by Ref. 33:

$$\alpha = \frac{1}{d} Ln\left[\frac{(1-R)^2}{T}\right] \quad (4)$$

where d is the thickness of the film and R and T are the reflectance and the transmittance, respectively.

The optical band gap (E_g) can be obtained by extrapolating the straight-line portion of $(\alpha h\nu)^2$ versus $h\nu$ plots to the energy axis.[34] The plots of $(\alpha h\nu)^2$ as a function of the incident photon energy $h\nu$

for GZO 3 at.% films deposited at various substrate temperatures are shown in Fig. 7. The deduced optical band gaps for films deposited at RT, 100°C, 200°C and 300°C are 3.63 eV, 3.57 eV, 3.65 eV and 3.48 eV, respectively. All the values are larger than that of pure bulk ZnO (3.30 eV). When the substrate temperature is increased, the value of E_g first decreases and then increases rapidly. This increase of the gap is caused by the Burstein–Moss effect,[35,36] which is related to the fact that the increased concentration of charge carriers block the lowest conduction band states (Burstein–Moss effect) and then transitions can occur only toward higher energy states.

Incorporatation of a higher doping concentration would induce the formation of band tails in the band gap, known as the Urbach tail of the films and expressed by Ref. 37 and 38

$$\alpha = \alpha_0 \exp\left(\frac{h\nu}{E_u}\right), \quad (5)$$

where α_0 is a constant and E_u is the Urbach energy, which refers to the optical transition between occupied states in the valence band tail and the conduction band edge.[37] The E_u values were obtained from the inverse of the slope of $Ln(\alpha)$ versus photon energy. The results are shown in Fig. 8. It has been demonstrated that the increase in the substrate temperature induces a decrease in the structural disorder decreases and an improvement of the stoichiometry.[39] Natsume et al.[40] have proposed an explanation for this variation in localized donor levels from interstitial zinc atoms states.

Zinc oxide is a transparent material whose refractive index in the bulk form is two.[41] In the case of thin films, the refractive index and the absorption coefficient vary depending on the conditions of preparation. The calculated refractive indices at different wavelengths are shown in Fig. 9. The refractive index has a value which varies between 1.80 and 2.40. The improvement in the stoichiometry of ZnO leads to a decrease of the absorption coefficient and an increase in the energy of the bandgap. The variation of the refractive index varies with the phonon energy for all the films and is shown in Fig. 9a. The refractive index of the samples decreases with the doping concentration. The observed variation of the refractive index with doping concentration for ZnO:Ga films can be explained on the basis of the contribution from both lattice contraction and the disorder of the films. This lowering of the refractive index can mainly be attributed to an increase of the carrier concentration in the ZnO film:Ga. Doping gallium in ZnO can act as an effective donor by substitutional introduction following Ga^{3+} Zn^{2+} in the place or incorporation of Ga ions in the interstitial spaces, generating free carriers. With increasing dopant concentration, the concentration of carrier in the ZnO film:Ga is increased. Therefore, the refractive index is decreased. From Fig. 9b, these variations indicate that the refractive index increases with the substrate temperature. This increase of the refractive index can be mainly attributed to an increase in carrier concentration in the films $Zn_{0.97}Ga_{0.03}O$.

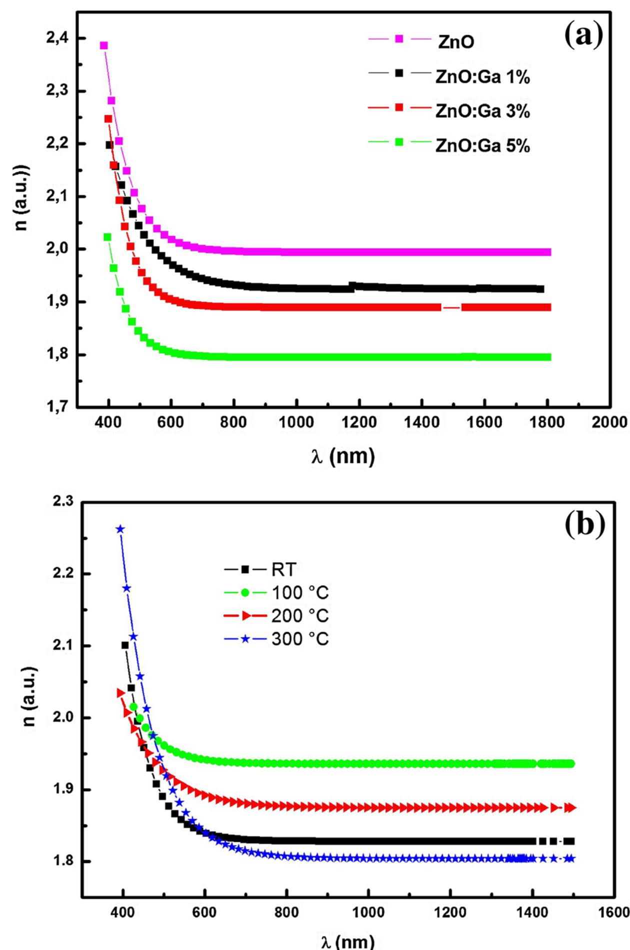

Fig. 9. Variation of refractive index with Ga concentration and substrate temperatures for GZO films as a function of wavelength.

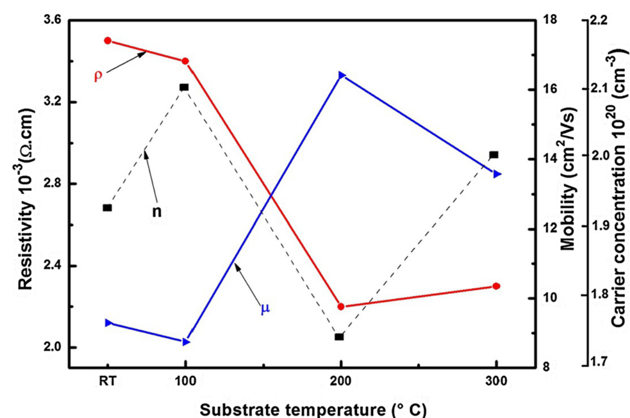

Fig. 10. Electrical properties for GZO 3.0 at.% films as a function of substrate temperature.

Table III. Electrical properties and band gap of ZnO:Ga films with different Ga contents and at different deposition temperatures

Temperature	Ga-doping level (content %)			
	0	1	3	5
RT				
$\rho(10^{-3}\ \Omega$ cm)	35.0	11.2	3.5	7.4
μ (cm^2/Vs)	4.12	5.87	9.30	4.93
n (10^{20} cm^{-3})	0.44	26.40	1.73	1.71
E_g (eV)	3.30	3.37	3.63	3.50
100°C				
$\rho(10^{-3}\ \Omega$ cm)	–	9.0	3.4	6.0
μ (cm^2/Vs)	–	6.67	8.87	6.64
n (10^{20} cm^{-3})	–	1.04	2.10	1.51
E_g (eV)	–	3.36	3.57	3.36
200°C				
$\rho(10^{-3}\ \Omega$ cm)	28.32	8.0	2.2	4.2
μ (cm^2/Vs)	5.38	7.30	16.42	10.19
n (10^{20} cm^{-3})	0.41	1.07	1.73	1.46
E_g (eV)	3.26	3.41	3.65	3.48
300°C				
$\rho(10^{-3}\ \Omega$ cm)	–	8.5	2.30	–
μ (cm^2/Vs)	–	7.58	13.85	–
n (10^{20} cm^{-3})	–	0.97	2.00	–
E_g (eV)	–	3.41	3.65	–

Electrical Studies

Figure 10 shows the electrical resistivity (ρ), carrier concentration (n) and mobility (μ) as function of substrate temperature. All our Hall measurement results, listed in Table III, of films are degenerately n-type semiconductors with a resistivity in the range of $10^{-3}\ \Omega$ cm. The films deposited at RT exhibit a resistivity of $3.50 \times 10^{-3}\ \Omega$ cm. As the substrate temperature increased to 200°C, the resistivity decreased to the minimum value of $2.20 \times 10^{-3}\ \Omega$ cm, and then slightly increased at 300°C, which is due to the improved Ga substitution and ZnO crystallinity at higher temperatures, as indicated by the XRD results. At this temperature, the mobility also undergoes a sharp increase, which results from the greatly weakened carrier scattering process due to the improvement of crystallinity. In addition, due to the polycrystalline nature of the film, higher substrate temperatures can promote desorption of oxygen from the grain boundaries,[42] which helps to promote Ga substitution and provides more donor states, thus increasing the mobility. The maximal mobility is 16.42 cm^2/Vs, which is obtained at 200°C. At this temperature, the mobility also undergoes an increase, which results from the greatly weakened carrier scattering process due to the improvement of crystallinity. The increase of electrical conductivity was attributed to better crystallinity of GZO film and its dense microstructure with somewhat larger grain sizes. The denser structure induced few pores, which behave as traps for free electrons and barriers for electrons transport in the film. Hence, a decrease in porosity associated with an increase in the grain size allows a decrease in election scattering, which leads to an increase in the conductivity. The increase in resistivity for temperatures above 200°C corresponds to a decrease in mobility. The most likely phenomenon explaining the decreased mobility is increased incorporation of impurities in the layers. The decrease in conductivity is attributed to an increase in chemisorbed oxygen, which acts as an electron trap and results in the decrease of carrier concentration,[43] while the decrease of carrier mobility may be related to the increase of grain boundary scattering for the free electrons. These results are in accordance with the theoretical explanation by Fu[44] and Hong et al.[45] Results of this study indicated that the conductivity of ZnO/Ga film was closely related to the crystallinity. The electrons resulted from small Ga donors (Ga_{Zn}). The electrical transport properties of ZnO:Ga films were dominated by the carrier concentration and mobility. V. Khranovskyy's results[46] indicated that the conductivity was strongly dependent on the crystallinity of Ga-doped ZnO film. However, the electrical transport properties of the films were dominated by either carrier concentration or mobility. While the weakening in crystallinity shows an increasing trend with substrate temperature at 300°C, possibly due to metal atoms in the grain boundaries, where they become inactive as donors and modify the potential barrier for charge transport across the grains, resulting in a resistiv-

ity increase.[47,48] At this temperature, the Hall mobility decreased from 16.42 $cm^2 V^{-1}s^{-1}$ to 13.58 $cm^2 V^{-1} s^{-1}$. This could be related to the segregation of Ga_2O_3 at the grain boundaries at high temperatures, which reduced the doping efficiency and increased the grain barrier scattering. Similar results have been reported for AZO thin films.[26–28] As a result, the resistivity of the GZO films reached the minimum value of 2.20×10^{-3} (Ω cm) at the substrate temperature of 200°C.

CONCLUSION

High-quality transparent GZO thin films were grown on glass substrates at various substrate temperatures by RF-magnetron sputtering, using aerogel nanopowder prepared by the sol–gel technique. The impact of the substrate temperature on the structural, electrical and optical properties of GZO films have been investigated. All films have a hexagonal wurtzite structure and a preferred orientation along the c-axis. It has been established that the effect of the substrate temperature modifies the film growth process and, hence, affects the structure and surface morphology. The GZO deposited layers have a low resistivity, with a minimum value of 2.2×10^{-3} Ω cm obtained for the sample deposited at a substrate temperature of 200°C. We found that the resistivity decreases with increasing the substrate temperature, and this decrease is caused by the improvement of crystallinity. In addition, all the layers are highly transparent in the visible range and show an increase of optical gap with increasing temperature. Based on the good conductivity and high transmittance, the GZO films prepared by RF-magnetron sputtering can be regarded as a transparent electrode.

REFERENCES

1. Z. Deheng, Z. Dejun, and W. Qingpu, *J. Mater. Sci. Technol.* 17, 517 (2001).
2. C.Y. Liu, B.P. Zhang, Z.W. Lu, N.T. Binh, K. Wakatsuki, Y. Segawa, and R. Mu, *J. Mater. Sci. Mater. Electron.* 20, 197 (2009).
3. H. Zeng, G. Duan, Y. Li, S. Yang, X. Xu, and W. Cai, *Adv. Funct. Mater.* 20, 561 (2010).
4. T. Reimer, I. Paulowicz, R. Röder, S. Kaps, O. Lupan, S. Chemnitz, W. Benecke, C. Ronning, R. Adelung, Y.K. Mishra, and A.C.S. Appl, *Mater. Interfaces* 6, 7806 (2014).
5. D. Gedamu, I. Paulowicz, S. Kaps, O. Lupan, and S. Wille, *Adv. Mater.* 26, 1541 (2014).
6. M. Hjiri, R. Dhahri, L. El Mir, A. Bonavita, N. Donato, S.G. Leonardi, and G. Neri, *J. Alloys Compd.* 634, 187 (2015).
7. A.E. Jiménez and J.A. Soto Urueta, *Sol. Energy Mater. Sol. Cells* 52, 345 (1998).
8. G.A. Hirata, J.M. Siqueiros, J.A. Diaz, O. Contreras, J. McKittrick, T. Cheeks, and O.A. Lopez, *Thin Solid Films* 288, 29 (1996).
9. R. Ayouchi, D. Leinen, F. Martı'n, M. Gabas, E. Dalchiele, and J.R. Ramos-Barrado, *Thin Solid Films* 426, 68 (2003).
10. K.Y. Cheong, N. Muti, and S. Roy Ramanan, *Thin Solid Films* 410, 142 (2002).
11. H. Gomez and M. De la Olvera, *Mater. Sci. Eng. B* 134, 20 (2006).
12. B.T. Lee, T.H. Kim, and S.H. Jeong, *J. Phys. D Appl. Phys.* 39, 957 (2006).
13. G.K. Paul and S.K. Sen, *Mater. Lett.* 57, 742 (2002).
14. P. Petrou, R. Singh, and D.E. Brodie, *Appl. Phys. Lett.* 35, 930 (1979).
15. B.M. Ataev, A.M. Bagamadova, A.M. Djabrailov, V.V. Mamedov, and R.A. Rabadanov, *Thin Solid Films* 260, 19 (1995).
16. J. Hu and R.G. Gordon, *J. Appl. Phys.* 72, 5381 (1992).
17. K.T.R. Reddy and R.W. Miles, *J. Mater. Sci. Lett.* 17, 279 (1998).
18. T. Minami, H. Sato, and S. Takata, *Jpn. J. Appl. Phys.* 24, 781 (1985).
19. L. El Mir, F. Ghribi, M. Hajiri, Z. Ben Ayadi, K. Djessas, M. Cubukcu, and H.J. von Bardeleben, *Thin Solid Films* 30, 5787 (2011).
20. H. Mahdhi, Z. Ben Ayadi, L. El Mir, K. Djessas, and S. Alaya, *Sens. Lett.* 9, 2150 (2011).
21. S.M. Park, T. Ikegami, and K. Ebihara, *Thin Solid Films* 513, 90 (2006).
22. G. Aygun and I. Yildiz, *J. Appl. Phys.* 106, 014312 (2009).
23. K. Omri, I. Najeh, R. Dhahri, J. El Ghoul, and L. El Mir, *Microelectron. Eng.* 128, 53 (2014).
24. Z. Ben Ayadi, L. El Mir, K. Djessas, and S. Alaya, *Nanotechnology* 18, 445702 (2007).
25. B.D. Cullity, *Elements of X-ray Diffraction* (Reading, MA: Addison-Wesley, 1978), p. 102.
26. W.Q. Peng, S.C. Qu, G.W. Cong, and Z.G. Wang, *Mater. Sci. Semicond. Process.* 9, 156 (2006).
27. K. Ellmer, R. Cebulla, and R. Wendt, *Thin Solid Films* 317, 413 (1998).
28. H. Deng, J.J. Russel, R.N. Lamb, and B. Jiang, *Thin Solid Films* 458, 43 (2004).
29. S. Mondal, S.R. Bhattacharyya, and P. Mitra, *J. Phys.* 80, 315 (2013).
30. M.-C. Jun, S.-U. Park, and J.-H. Koh, *Nanoscale Res. Lett.* 7, 639 (2012).
31. H. Mahdhi, Z. Ben Ayadi, J.L. Gauffier, K. Djessas, and S. Alaya, *Opt. Mater* 45, 97 (2015).
32. J. Tauc, *Mater. Res. Bull.* 3, 37 (1968).
33. S. Belgacem and R. Bennaceur, *Rev. Phys. Appl.* 25, 1245 (1990).
34. J. Tauc, R. Grigo Rovici, and A. Vancu, *Phys. Status Solidi* 15, 627 (1966).
35. E. Burstein, *Phys. Rev.* 93, 632 (1954).
36. T.S. Moss, *Phys. Soc. Lond. B* 67, 775 (1954).
37. S. Aksoy, Y. Caglar, S. Ilican, and M. Caglar, *J. Alloys Compd.* 512, 171 (1992).
38. Y. Caglar, M. Caglar, and S. Ilican, *Curr. Appl. Phys.* 12, 963 (2012).
39. N.R. Aghamalyan, I.A. Gambaryan, E.K. Goulanian, R.K. Hovsepyan, R.B. Kostanyan, S.I. Petrosyan, E.S. Vardanyan, and A.F. Zerrouk, *Semicond. Sci. Technol.* 18, 525 (2003).
40. Y. Natsume and H. Sakata, *Thin Solid Films* 372, 30 (2000).
41. R.C. Weast, *Handbook of Chemistry and Physics*, 56th ed. (Cleveland, OH: CRC Press, 1975), p. B-204.
42. Q.-B. Ma, Z.-Z. Ye, H.-P. He, J.-R. Wang, L.-P. Zhu, and B.-H. Zhao, *Vacuum* 82, 9 (2008).
43. J.F. Chang and M.H. Hon, *Thin Solid Films* 386, 79 (2001).
44. E.G. Fu, D.M. Zhuang, G. Zhang, and W.F. Yang, *Appl. Surf. Sci.* 217, 88 (2003).
45. R.J. Hong, X. Jiang, B. Szyszka, V. Sittinger, and A. Pflug, *Appl. Surf. Sci.* 207, 341 (2003).
46. V. Khranovskyy, U. Grossner, O. Nilsen, V. Lazorenko, G.V. Lashkarev, B.G. Svensson, and R. Yakimova, *Thin Solid Films* 515, 472 (2006).
47. F. Wang, M.Z. Wu, Y.Y. Wang, Y.M. Yu, X.M. Wu, and L.J. Zhuge, *Appl. Phys. A* (2012). doi:10.1016/j.Vacuum02.040.
48. C. Guillen and J. Herrero, *Vacuum* 84, 924 (2010).